Geostatistical normalization of air pollution transport model output and station data using Isatis

H. WACKERNAGEL

IMPACT Project Report No 4 (Contract IST-1999-11313)

December 2002

Technical Report N–20/02/G
ENSMP - ARMINES, Centre de Géostatistique
35 rue Saint Honoré, F-77305 Fontainebleau, France
http://cg.ensmp.fr

Contents

Summary

This report[1] is Deliverable 4 of the EC funded "IMPACT" IST project on "*Estimation of Human Impact in Presence of Natural Fluctuations*[2].

The geostatistical software *Isatis*[3] is presently used by around forty air pollution monitoring agencies in France and abroad[4]. It is thus of interest to provide the practical implementation details with Isatis of aspects of the Paris area ozone case study that were treated in several other IMPACT Project reports [9, 8, 10, 1, 5].

The report is divided into two parts. The first part (Chapter 1) shows how to correct by kriging the output of a chemical transport model with the help of measurements from air pollution stations. The second part (Chapter 2) uses the corrected transport model output and a geostatistical change-of-support model gained from the station data to evaluate the proportion of territory above alert level at a smaller spatial scale than that provided by the transport model. The conclusions are summarized in Chapter 3.

[1]The report is available as a pdf file and is best viewed with the Acrobat-reader, which allows to take full advantage of the internal and external links.

[2]See the IMPACT Project Website: http://www.mai.liu.se/impact/.

[3]*Isatis* is a trademark of Transvalor.

[4]Information about Isatis can be obtained at the sites of Geovariances: http://www.geovariances.fr or http://www.geovariances-americas.com.

Chapter 1

Kriging with Chimere external drift

In this first part the Chimere transport model output is used to capture the non-stationarity of a probabilistic model which postulates the presence of an ozone plume NW of Paris on a summer day of 1999. The spatial covariance is determined by fitting the variogram in a direction that is less affected by the non-stationarity. New values of hourly ozone are computed for the Paris area using Airparif measurements in a kriging guided by the Chimere output.

1.1 Airparif station data and Chimere transport model

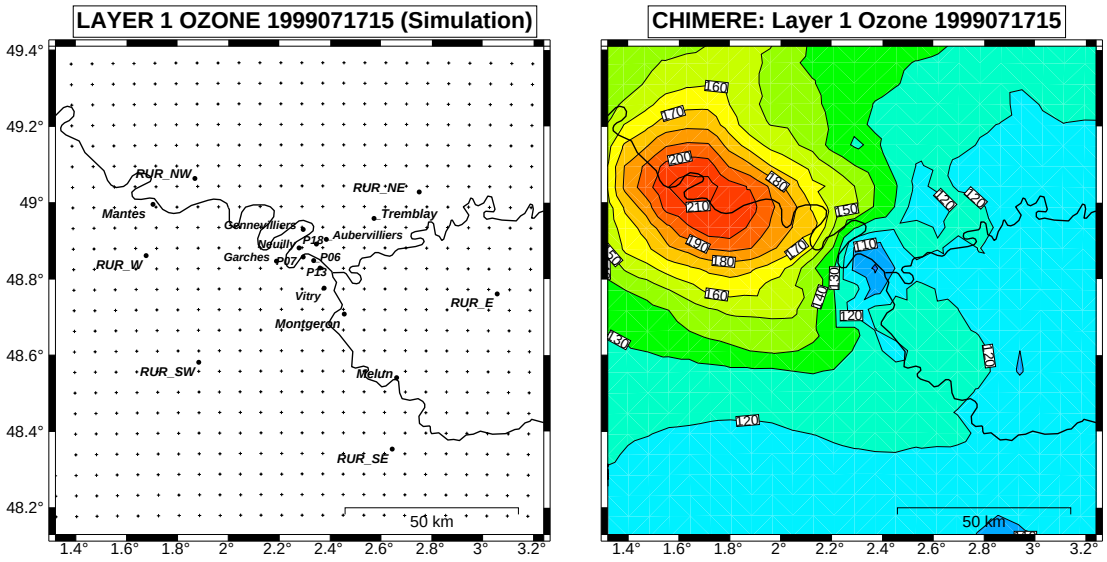

Figure 1.1: On the left: location of the 19 Airparif background stations and of the 25×25 Chimere grid nodes. On the right: Chimere transport model ozone predictions for 17 July 1999 at 15 hours UT.

The station data from the area around Paris (called *Ile de France*) has been provided to us by the Airparif association and it can be downloaded on its site[1]. The output from the chemical transport model Chimere [13, 12] was kindly sent to us by Nadège Blond from the air quality research team of the Laboratoire de Météorologie Dynamique, who has extensively studied data assimilation and mapping problems in her recent thesis [3]. The ESQUIF project proposes an extensive data base of Paris area air pollution data: http://climserv.lmd.polytechnique.fr/esquif/.

The Airparif data was delivered in Lambert II coordinates which were transformed into longitudes and latitudes at the WEB site of the Institut für Photogrammetrie und Fernerkundung (University of Karlsruhe). The Chimere output was in latitude and longitude coordinates.

The map of the 19 Airparif background station locations and the 25×25 Chimere grid nodes is displayed on the left of **Figure 1.1**. We notice that six stations are characterized as *rural* (with names beginning by "*RUR*"). We also notice that almost half of the stations are clustered in downtown Paris.

The map of Chimere transport model ozone predictions for 17 July 1999 at 15 hours UT (which corresponds to 17 hours Paris summer time) is shown on the right of **Figure 1.1**. We see that the ozone plume is located NW of the urban area on this day characterized by stagnant weather (wind speed: 3 m/s at Roissy airport).

The maps have been generated with the public domain software GMT[2] which allows for many different geographic projections. On both maps the two main rivers have been plotted: the Marne and the Seine river, where the first flows from East into the latter, a little upstream from Paris.

The coordinates for the geostatistical study have been obtained by a linear projection of the longitude and latitude coordinates using the GMT command:

```
mapproject COORD -R1.32/3.24/48.13/49.41 -JX150/150d
```

where `COORD` is a coordinates file, the parameter `-R` describes the region in longitude and latitude coordinates and the parameter -JX indicates the size of the area in km. The resulting Chimere grid is not perfectly orthogonal.

[1] Airparif association: http://www.airparif.asso.fr.

[2] GMT (*Generic Mapping Tools*) is downloadable at: http://gmt.soest.hawaii.edu/.

1.2 Input of data into Isatis and definition of grid

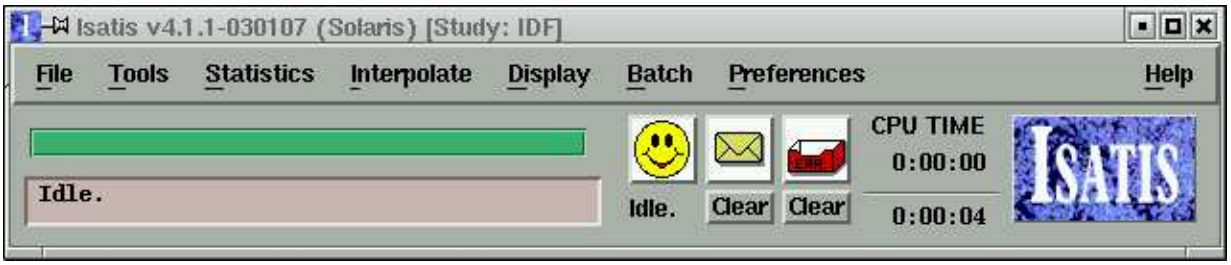

Figure 1.2: The Isatis main window.

Isatis, whose main window is displayed on **Figure 1.2**, is a general purpose geostatistical software package that has presently been adopted by forty air pollution monitoring associations in France and abroad.

The data in Isatis ASCII-format is contained in the two files IdfSTA17_29jul15h.isa and IdfCHIM17_29jul15h.isa. The ozone measurements at the stations are stored in the variable "`Ozone`" while the Chimere predictions receive the name "`O3`".

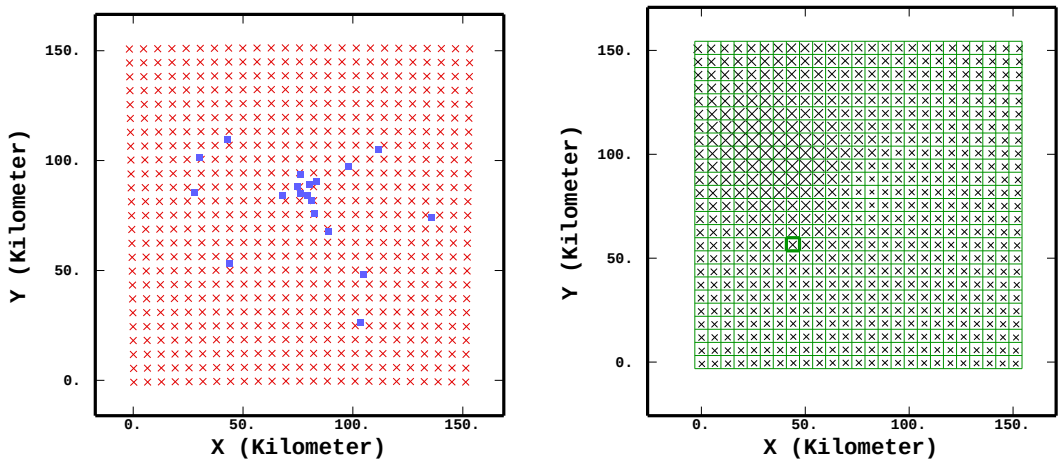

Figure 1.3: On the left, the locations of the Airparif stations (blue squares) and the Chimere grid nodes (red crosses). On the right, the Chimere grid nodes (black crosses) and square grid cells (in green) of size 6.3×6.3 km^2.

The **Figure 1.3** shows on the left a display of the locations of the Airparif stations (blue squares) and the Chimere grid nodes (red crosses). On the right, the Chimere grid nodes (black crosses) are displayed together with orthogonal grid cells of size 6.3×6.3 km^2. The origin of that grid coincides with the origin of the coordinate system. Each Chimere grid node lies within one square grid cell.

The estimation of the ozone values at the center of the square grid cells will be performed by kriging the station values including Chimere predictions as external drift.

1.3 Migrating Chimere output to kriging grid and to stations

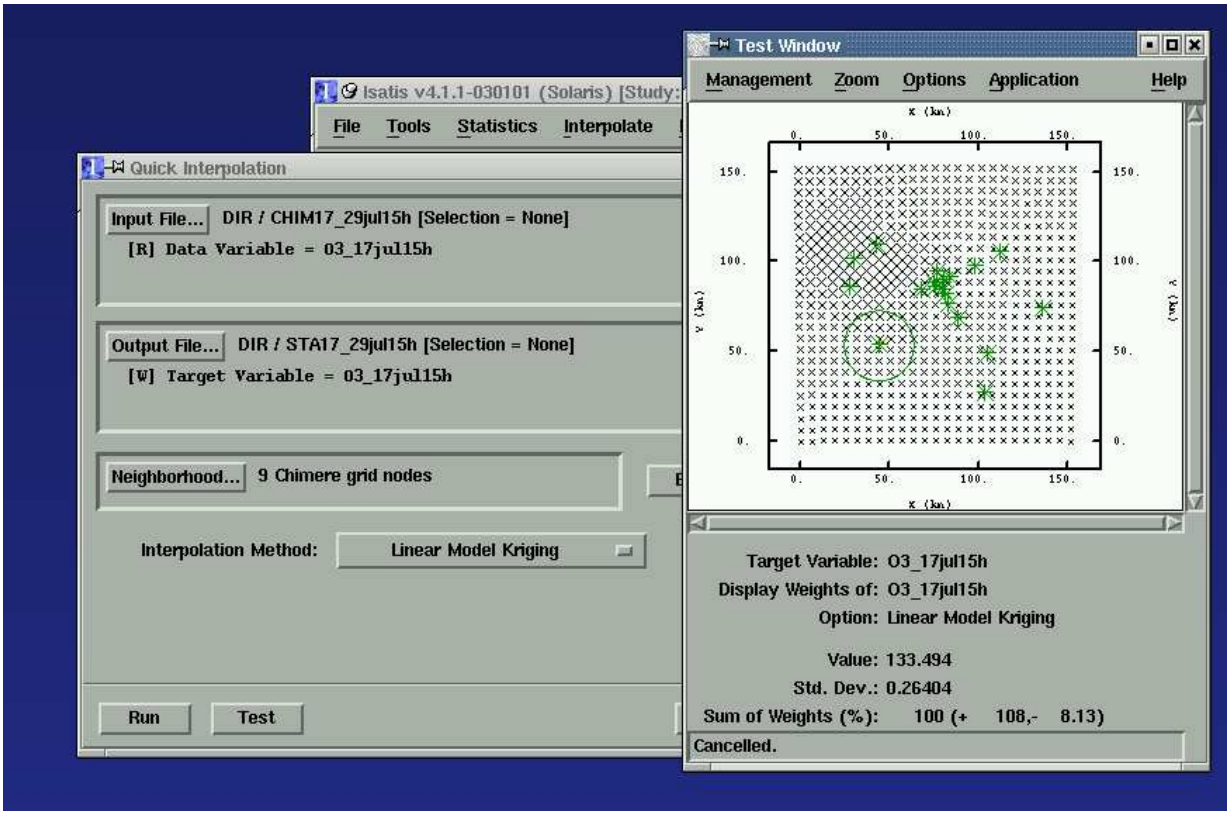

Figure 1.4: Neighborhood radius for interpolating Chimere output at a RUR_SW station.

For external drift kriging we need the Chimere values both at the kriging grid nodes and at the station locations.

Each Chimere value has been migrated to the center of the kriging grid cell in which it lies. There are two ways of doing this in Isatis. One way is to use:

`Tools` ↦ `Migrate` ↦ `Points -> Grid`

The second way, which we chose, is to use an ordinary kriging with only one point in the neighborhood, because the constraint of unit sum weights implies a unit weight and so ordinary kriging will transfer the unique value in the neighborhood to the estimation location. The result is identical to the `migrate` menu. A simplified implementation of ordinary kriging is found in:

`Interpolate` ↦ `Quick Interpolation`

selecting `Linear Model Kriging` (default) and a `moving` neighborhood with only one point. The variogram model used in that automatic interpolation is a linear model with unit slope (the value of the slope parameter has no effect on interpolation weights).

The value of Chimere output at a station location was set in a different way. We decided to take a weighted moving average of the nine nearest points and used again ordinary kriging in the `quick interpolation` implementation, as above. The search radius was set wide enough to include the nine nearest points in the neighborhood.

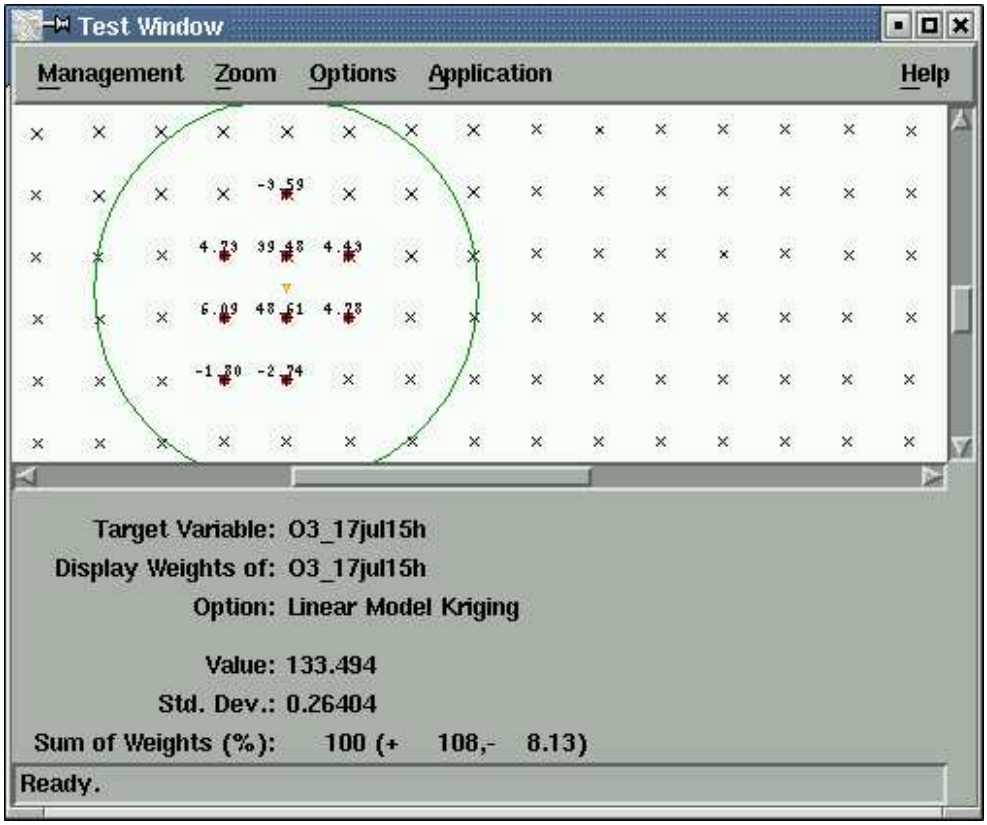

Figure 1.5: Interpolation of Chimere output at a RUR_SW station.

The neighborhood used is displayed on **Figure 1.4**: the circle around the station RUR_SW represents the search radius. The nine Chimere nodes selected can be seen on **Figure 1.5**. Next to each node we see the interpolation weight (which may be negative in ordinary kriging due to screen effect, see [15]). The RUR_SW station happens to be located almost halfway between two Chimere nodes so that the interpolation weights for the node values are 48.6% and 39.5%, representing 88% of the total weight. The sum of negative weights amounts only to -8%. The interpolated value is 133.5 μg/m^3 while the Airparif measurement is 171 μg/m^3 at the RUR_SW station[3]. The reported kriging standard deviation `Std.Dev.` is meaningless because the vari-

[3]Such discrepancies are not exceptional as will be seen when discussing the overall statistics and in particular

ogram was not fitted to data.

1.4 Statistics of Chimere predictions and station data

We compare the statistics of the ozone values of the Chimere predictions and the Airparif measurements whose histograms are displayed on **Figure 1.6**.

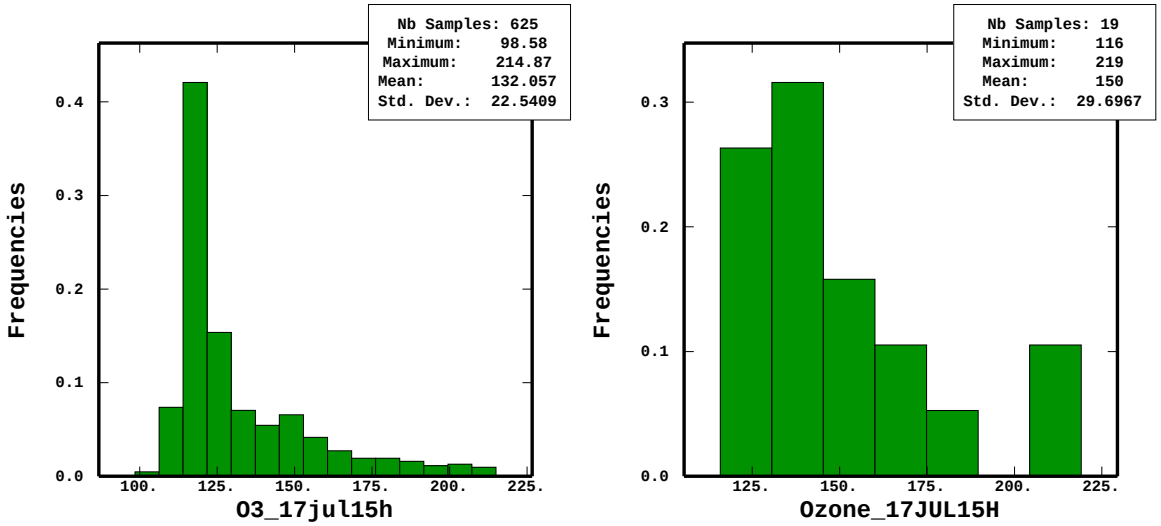

Figure 1.6: Histograms of the Chimere predictions (left) and the Airparif measurements (right) of Paris ozone on 17 July 1999 at 15UT.

The mean of Chimere, 132 μg/m^3 is lower than that of the measurements, which is 150 μg/m^3. The extremes (minima, maxima) are also lower. Can we conclude that Chimere underestimates the ozone? This is not clear for two reasons:

- the *sampling* locations of the Airparif stations is preferential, with a cluster of stations in downtown Paris, and so the region is very unevenly covered by the 19 samples.
- the *spatial support* is very different, with Chimere values representing hourly average over a 40km^2 cell while the Airparif stations measure the average air mass passing at a point during one hour.

The standard deviation of 22 μg/m^3 for Chimere is lower than the standard deviation of 30 μg/m^3 for the stations. This is consistent with the larger spatial support of Chimere.

The **Figure 1.7** displays the correlation diagram between the Chimere predictions (abscissa) and the station data (ordinate). The values of the 4 stations lying E and SE of Paris have been marked in green as they single out. The 3 stations within the plume W of Paris also single out as the highest values. The remaining 12 values form a cloud of points above the bisector.

Figure 1.7.

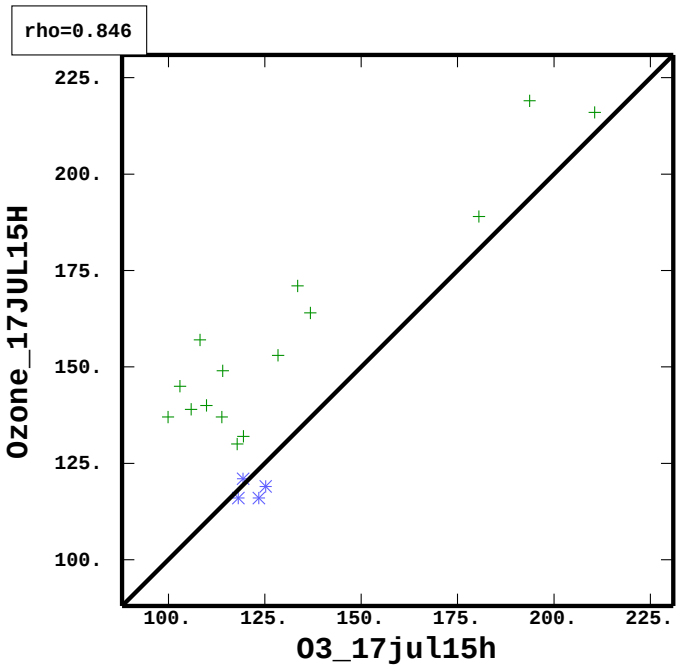

Figure 1.7: Correlation diagram between the Chimere predictions (abscissa) and the station data (ordinate).

1.5 Experimental variogram of station data

The experimental variogram consists in calculating the average of squared differences of pairs of sample values for distance and angle classes. It has been computed into two directions: 50 and 140 degrees with a tolerance of ± 20 degrees. The variograms into the two directions, labeled "`D1`" and "`D2`" are shown on the left of **Figure 1.8**. The squared difference between the ozone values of each sample pair are plotted as green crosses. The values of the experimental variogram are plotted with green dots joined by line segments and the number of pairs used for calculating each variogram value is written above the dot. The distance class width is 5km: each dot is plotted at the average distance of the pairs in each class and when no pair is found it is not plotted.

With 19 partly clustered samples the computation of two directions yields a very small number of pairs in those classes that are not empty. The three last classes for `D1` each contain only one pair and the experimental variogram in that direction is plotted without them on the right of **Figure 1.8**.

It is remarkable how the variogram computed into the direction `D2` in which Chimere postulates a plume (on the basis of meteorology and emissions) is singled out by the experimental variogram calculation. An indication that Chimere might be right. One possible interpretation is that the quadratic increase of the variogram in direction `D2` is due to the presence of the plume

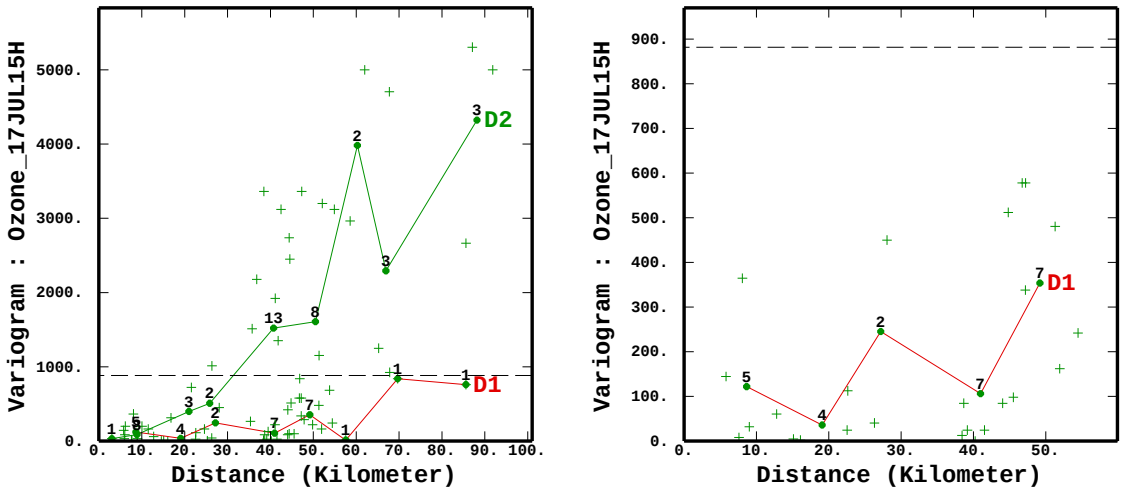

Figure 1.8: On the left: the experimental variogram of the 19 station ozone measurements computed into two directions `D1` and `D2`. On the right: the variogram in direction `D1` omitting the last three distance classes.

and that the variogram in direction `D1` describes additional variation not related to the formation of the plume. In geostatistical terms we would say that the direction `D1` gives us access to the underlying variogram. In this spirit we are going to adopt a model similar to the one used for kriging January temperatures in Scotland [7, 15] where elevation was used as external drift.

1.6 Variogram model and kriging with external drift

The non-stationary model adopted for the station measurements is that $Z(\mathbf{x}) = m(\mathbf{x}) + Y(\mathbf{x})$. The variogram of the isotropic random function $Y(\mathbf{x})$ is determined by fitting the experimental variogram into direction `D1`. The non-stationarity $m(\mathbf{x})$ is assumed to be linearly related to the Chimere output $s(\mathbf{x})$ by the relation $m(\mathbf{x}) = a + b\,s(\mathbf{x})$ where the coefficients a and b will actually be implicitly[4] estimated by the kriging with external drift.

The variogram in direction `D1` was fitted with a spherical variogram with a sill of 500 and a range of 100km and is shown on the right of **Figure 1.9**. The sill, with a value inferior to the variance of 881 (dashed line on the graphs), represents part of the variability, which is also explained by the drift. The range was chosen arbitrarily. This isotropic point variogram model is used in a kriging where the point station data serves to estimate the $6.3\times6.3\text{km}^2$ kriging grid cells. For the computation of the point-cell covariances in the right hand side of the kriging system we used a 5×5 discretization of the cells. The Chimere ouput is introduced into the

[4]The external drift coeffi cients can be computed explicitly by modifying the right hand side of the kriging system. However they are presently not provided by Isatis.

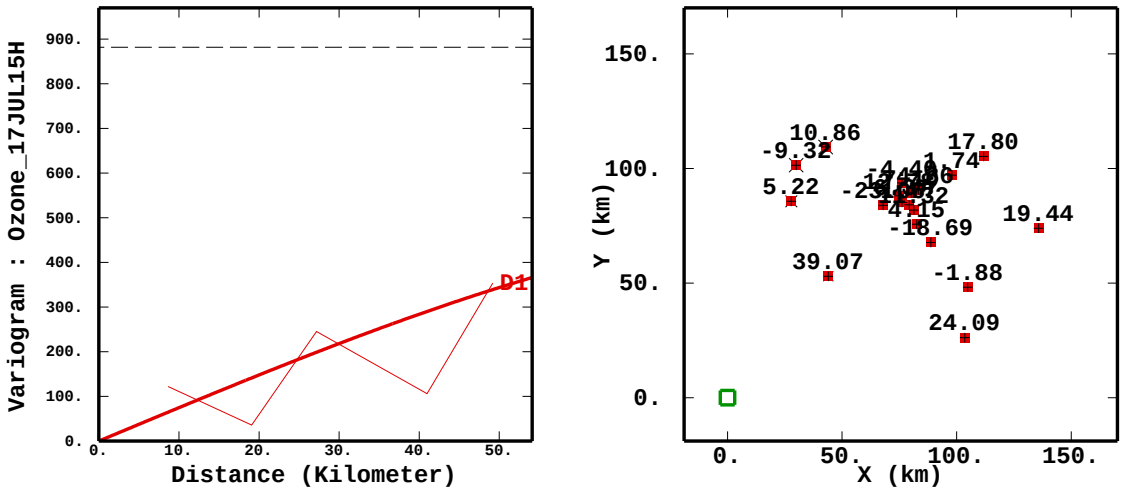

Figure 1.9: On the left, the fit of the variogram in direction `D1` by a spherical model with a sill of 500 and a range of 100km. On the right, the weights for the kriging with external drift of the cell centered at the origin.

kriging in the form of an additional constraint (external drift) and merely helps to shape the mean function.

Conversely we can say, as we are producing results on the same support as Chimere, that the external drift kriging delivers a new version of the Chimere output corrected by the station data.

Merely for illustration, the weights for the kriging with external drift (KED) of the cell centered at the origin are displayed on the right of **Figure 1.9**. The `RUR_SW` and the `RUR_SE` stations share 63% of positive weight[5]. It is actually remarkable that five stations lying at the border of the sampled domain (`RUR_NW, RUR_NE, RUR_E, RUR_SE, RUR_SW`) share 111% of positive weight. The total of negative weights, mainly concentrated in the central cluster, amounts to -62% and is symptomatic of the strong influence of the Chimere drift.

The Isatis window for estimating the Chimere cell averages from station data with external drift is displayed on the left of **Figure 1.10**. The type of calculation is `block` kriging. As input at station locations (file: `STA`) we have the measurements (variable: `Ozone`) and the Chimere values (variable: `O3`). As input at the kriging grid nodes (file: `GRID`) we have also Chimere values (variable: `O3`). As output we created at the kriging nodes (file: `GRID`) two new variables `Ozone` and `ERR_Ozone`. The fitted variogram model was named "`StationsDir1`" and the neighborhood for kriging consists of all 19 stations "(`Unique Nbhd`"). We need to edit the model and to specify within that Isatis window (displayed on the right of **Figure 1.10**) that the random function model includes an external drift by setting `basic drift functions` to the value: "`1 f1`".

[5]The total weight is 100% and is composed of the sum of the positive and the negative weights.

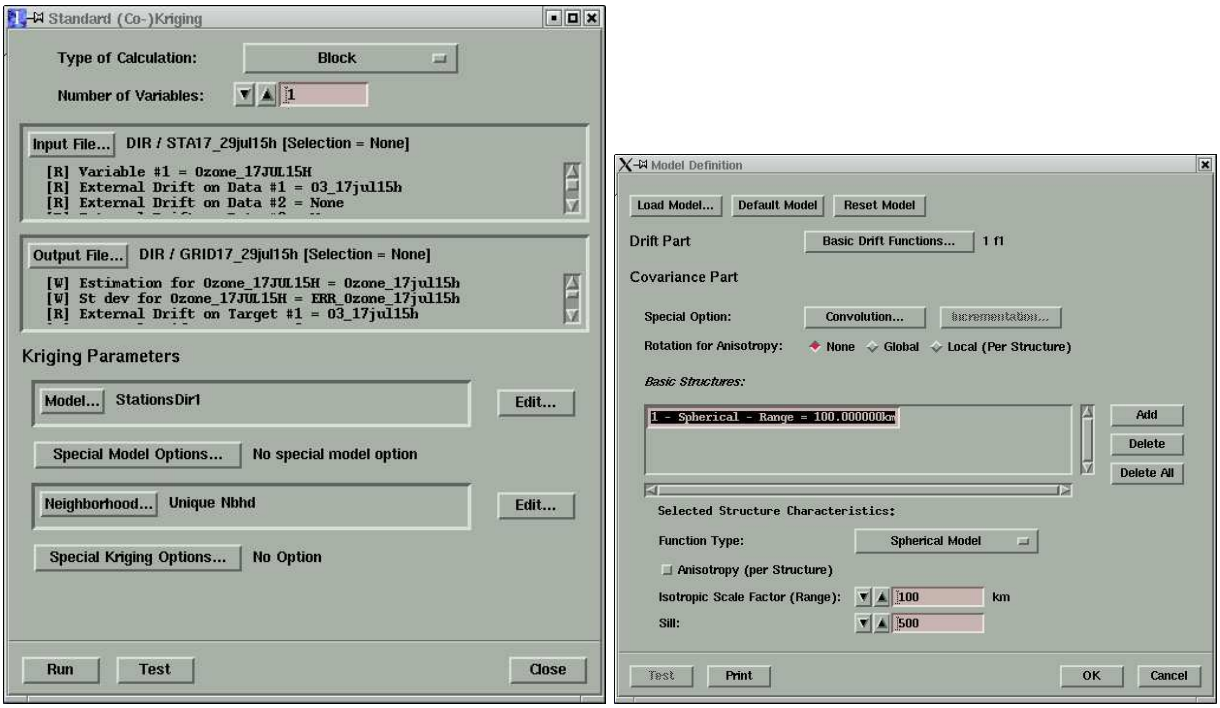

Figure 1.10: Isatis window set for kriging the Chimere cells by KED (left). The model is edited for adding the external drift (right).

The contoured map of the cell values estimated by KED and the corresponding kriging standard deviation are displayed on **Figure 1.11**. The histogram of the KED values is shown on the left of **Figure 1.12** and comparing the statistical parameters with those of the Chimere output on **Figure 1.6** we see that KED has raised the mean from 132 to 149 μg/m^{3}and the standard deviation from 23 to 25; the minimum was raised from 99 to 109 μg/m^{3}and the maximum from 215 to 222 μg/m^3. The histogram classes of KED are poorly contrasted as compared to the sharply left skew shape of the Chimere ouput. The scattergram on the right of **Figure 1.12** between the Chimere output (abscissa) and the KED values (ordinate) has a shape that resembles the scattergram between Chimere output and station data (**Figure 1.7**); the correlation coefficient has increased from .82 to .90.

1.7 Using a different variogram model

Due to the arbitrariness in the variogram model fitting, we propose an alternate variogram model with a shorter range (50km instead of 100km), a smaller sill (300 instead of 500) and a small discontinuity at the origin, i.e. a nugget-effect (10). This model is shown on the left of **Figure 1.13**. On the right of that figure we display the KED weights obtained for kriging the cell in the lower left corner of the kriging grid. In comparison with **Figure 1.9** the total of negative weights has

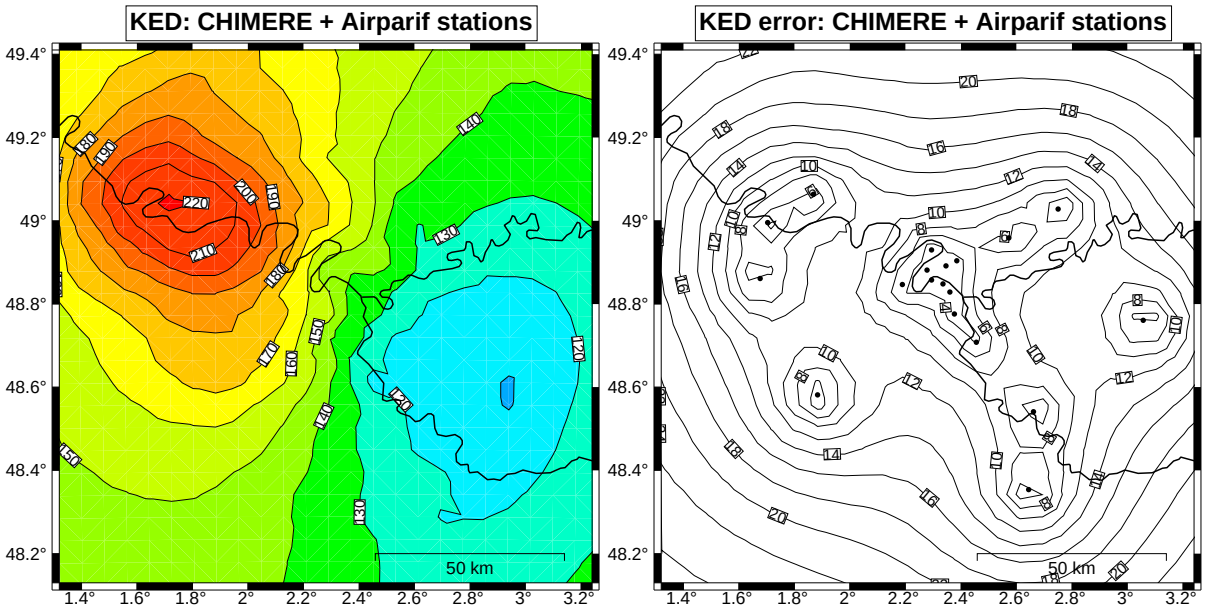

Figure 1.11: Contoured map of the cell values estimated by KED (left) and of the corresponding kriging standard deviation (right) using a spherical variogram model with a range of 100km.

gone down from -62% to -17%, which is mainly due to the inclusion of nugget-effect into the variogram model (and not to the reduction by half of the range). The contrast between the main weights is less sharp and overall this system of weights has less extrapolative power[6].

The contouring of the kriged values obtained with this new variogram model is displayed on **Figure 1.14** together with the corresponding kriging standard deviation. The bump of the plume is steeper and the kriging standard deviation lower (as compared with **Figure 1.11**). The histogram of kriged values is shown on **Figure 1.15** together with the scatter diagram against the Chimere output. The histogram is more contrasted than for the previous kriging and the scattergram has a more linear shape (as the one on **Figure 1.12**).

We will keep the results of this second KED for further calculations.

[6]Remember that in ordinary kriging (without drift) with a variogram model consisting of a pure nugget effect (white noise) equal to the variance 881, all weights would be equal to 5.3% and the estimated value at the lower left corner cell would be equal to the mean 150μg/m^3 with a kriging standard deviation of $\sqrt{\sigma^2/n}$), i.e. $\sqrt{881/19}$=6.8. The less structure in the variogram, the less contrasted is the system of weights. In the present KED problem, using a pure nugget-effect effect model would bring the total of negative weights down to less than 1% while the KED standard deviation would be 7.3%.

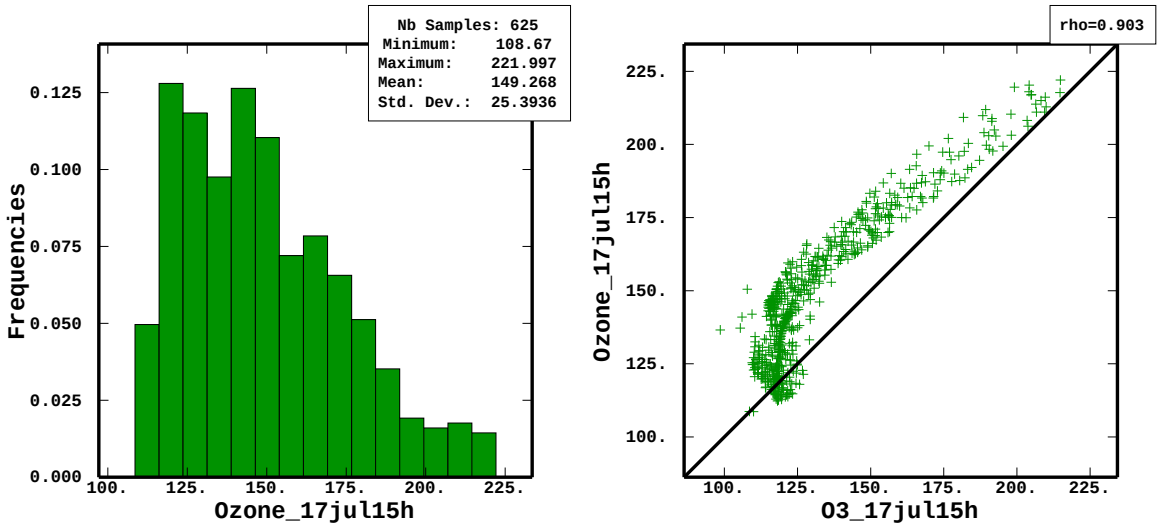

Figure 1.12: Histogram of the KED values displayed on Figure 1.11, on the left. Scattergram between Chimere output (abscissa) and KED values (ordinate), on the right.

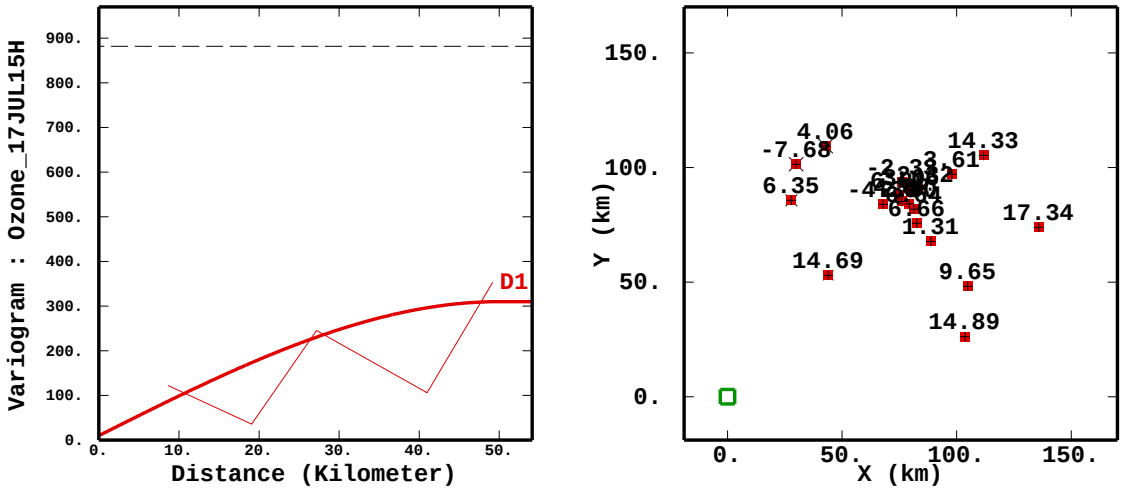

Figure 1.13: On the left, the fit of the variogram in direction `D1` by a model composed of a nugget effect of 10 plus a spherical model with a sill of 300 and a range of 50km. On the right, the weights for the kriging with external drift of the cell centered at the origin.

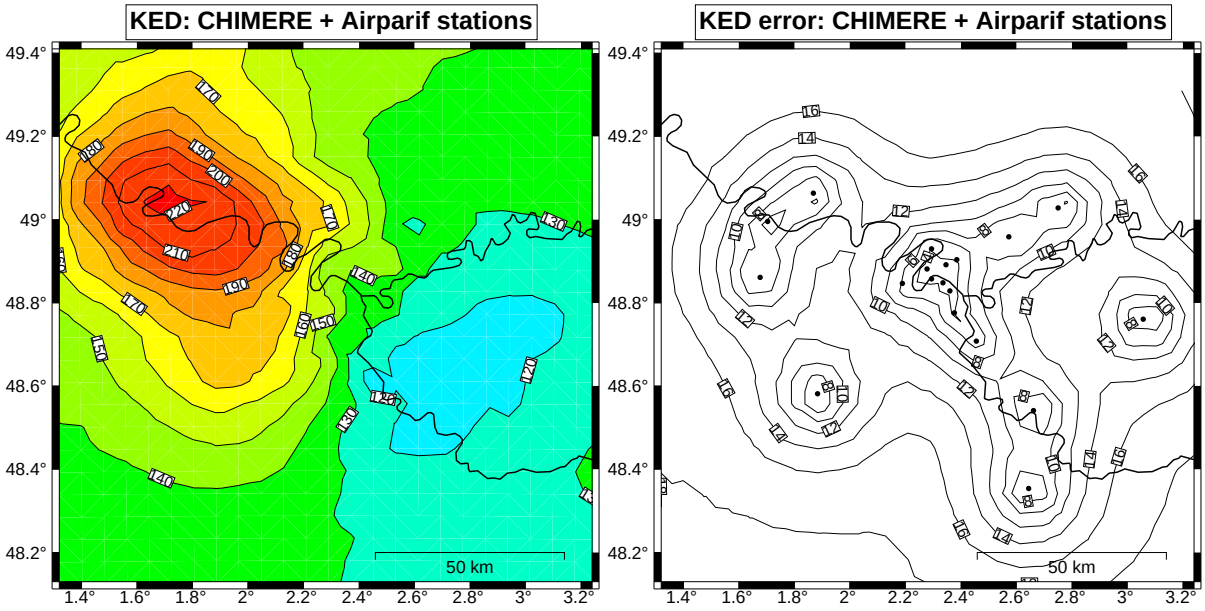

Figure 1.14: Contoured map of the cell values estimated by KED (left) and of the corresponding kriging standard deviation (right) using a nugget effect and a spherical model with a range of 50km.

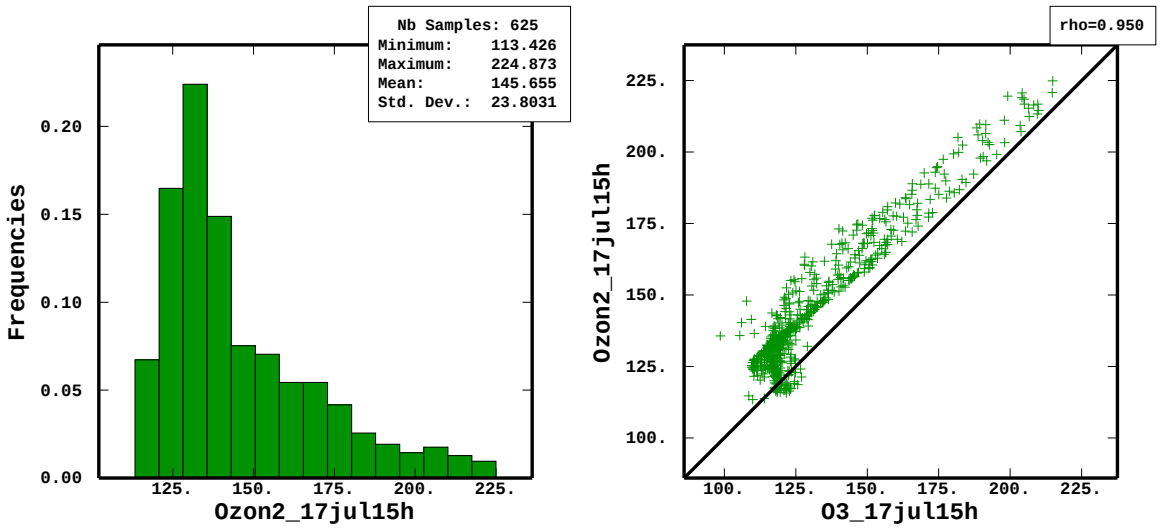

Figure 1.15: Histogram of the KED values displayed on Figure 1.14, on the left. Scattergram between Chimere output (abscissa) and the KED values (ordinate), on the right, for a nugget effect and a spherical model with a range of 50km.

Chapter 2

Uniform conditioning with Chimere

In this second part of the case study we take a different point of view. We will use the Chimere external drift kriging results for conditioning estimates of the proportion of blocks above alert level at a smaller scale of square kilometer size. As our change-of-support model relies on the distribution of the values over the whole domain, we will need to assume stationarity of the moments of all orders (strict stationarity).

2.1 Variogram of station data and declustering

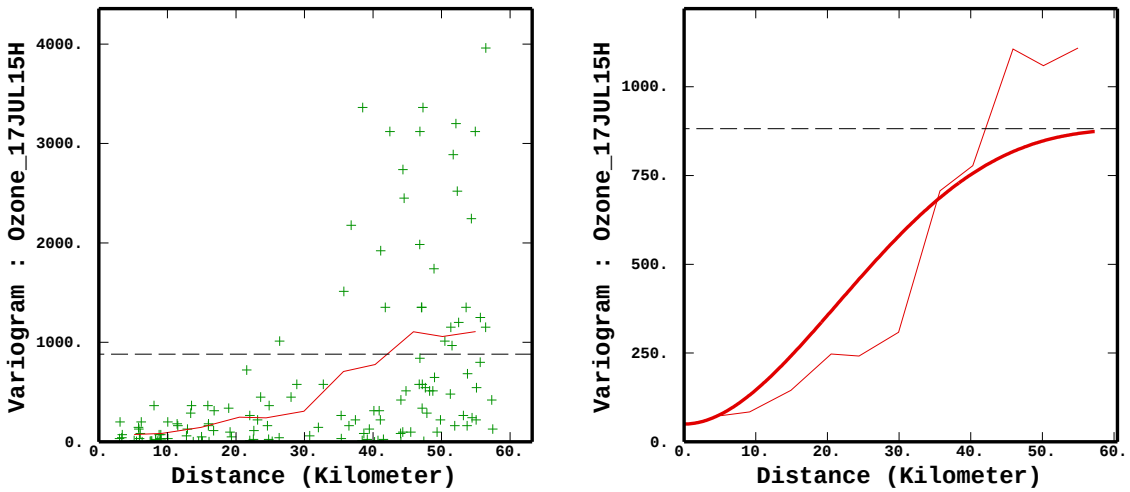

Figure 2.1: Omnidirectional experimental variogram (left). Fitted cubic model of range 70km with a sill of 831 plus a nugget effect of 50 (right).

We model the variogram in order to use it for computing dispersion variances in the change-of-support model. The omnidirectional experimental variogram is displayed together with the

variogram model on **Figure 2.1**[1]. The variogram has been fitted with a cubic model of range 70km with a sill of 831 and a nugget effect of 50, so that the total sill equals the variance of 881.

The cluster of data in downtown Paris provides a biased picture of the distribution and in particular of the variance. Isatis provides a declustering tool that we apply with a window of 40×40 km^2. This has the effect that the variance increases from 881 to 1228 while the mean decreases from 150 to 149 μg/m^3.

The declustering weights for the samples were saved under the name `weightsDC` for use in the anamorphosis. The point variogram total sill will be readjusted to be compatible with the new value of the variance.

2.2 Point-block-cell change-of-support model

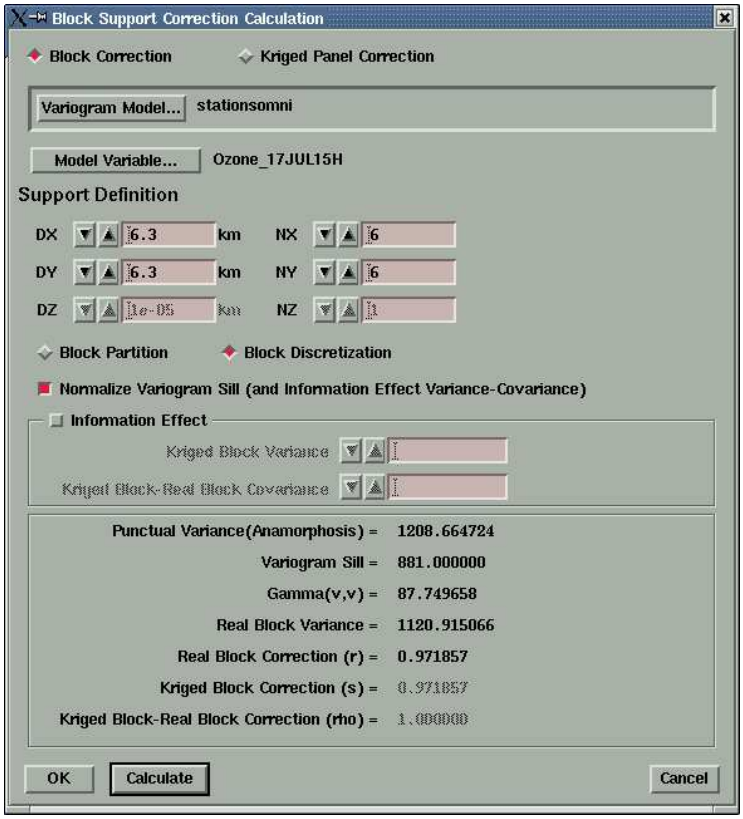

Figure 2.2: Isatis window for the 1×1 km^2 block support correction.

[1]The variogram cloud displays more points than on **Figure 1.8** because only the pairs entering the calculation of the experimental variogram are plotted. For the two directional variograms of **Figure 1.8** we had used a tolerance of ±20 degrees and omitted on purpose pairs in intermediate directions. We would need a tolerance of ±45 to include all pairs for two orthogonal directions.

We establish a change-of-support model for the station data considered as points, the Chimere cells of 6.3×6.3 km^2 and an intermediate spatial surface unit obtained by subdividing the cells into 6×6 blocks of square kilometer size. The basic motivation is the idea that square kilometer units provide a reasonably small *spatial decision unit* as compared to the 36 times larger Chimere cells.[2]

The point *anamorphosis*[3] with 30 Hermite polynomials slightly reduces the experimental variance so that we are actually working with a point variance of 1209 (instead of 1228 obtained after declustering). The variance of the blocks in the change-of-support model is then 1140 with a *point-block correlation* coefficient `r` = .97. The corresponding Isatis window is displayed on **Figure 2.2** and the results of the block anamorphosis are stored in a parameter set named "`1.05by1.05 blocks`". The *point-cell correlation* coefficient has the value `r` = .72.

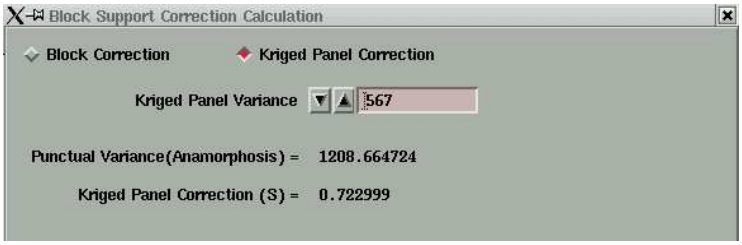

Figure 2.3: Isatis window for the 6.3×6.3 km^2 cell support correction.

The KED estimates of Section 1.7 for the Chimere cells have a variance of 567. This value is entered as the `panel variance` in the corresponding Isatis window shown on **Figure 2.3** (obtained by selecting `kriged panel correction` instead of `block correction`).

The **Figure 2.4** displays the Isatis main anamorphosis window,

`Statistics` $\mapsto$ `Gaussian Anamorphosis Modelling`

from which the subwindow **Figure 2.2** (or equivalently **Figure 2.3**) is generated when pressing the button `calculate`. The results of the cell anamorphosis are stored in a parameter set named "`6.3by6.3 panels`".

The plots showing the point-block and the point-cell anamorphosis (in red) as compared to the point anamophosis (in black) fitted to the empirical anamorphosis (staircase function) are found on **Figure 2.5**. They were obtained by pressing on the left icon of the Isatis window on **Figure 2.4**.

[2]Spatial decision units are, to our knowledge, not mentioned in air pollution regulations. Yet the problem is the same as for specifying the time support, which is explicited in most of these regulations: an alert threshold varies depending on whether e.g. 1h, 4h, 8h or 24h averages are considered. The larger the averaging time interval, the lower should be the alert level (which is generally the case, see [4], p19–20, p73–74) .

[3]A detailed description of Gaussian anamorphosis modeling with Hermite polynomials is found in [2, 15].

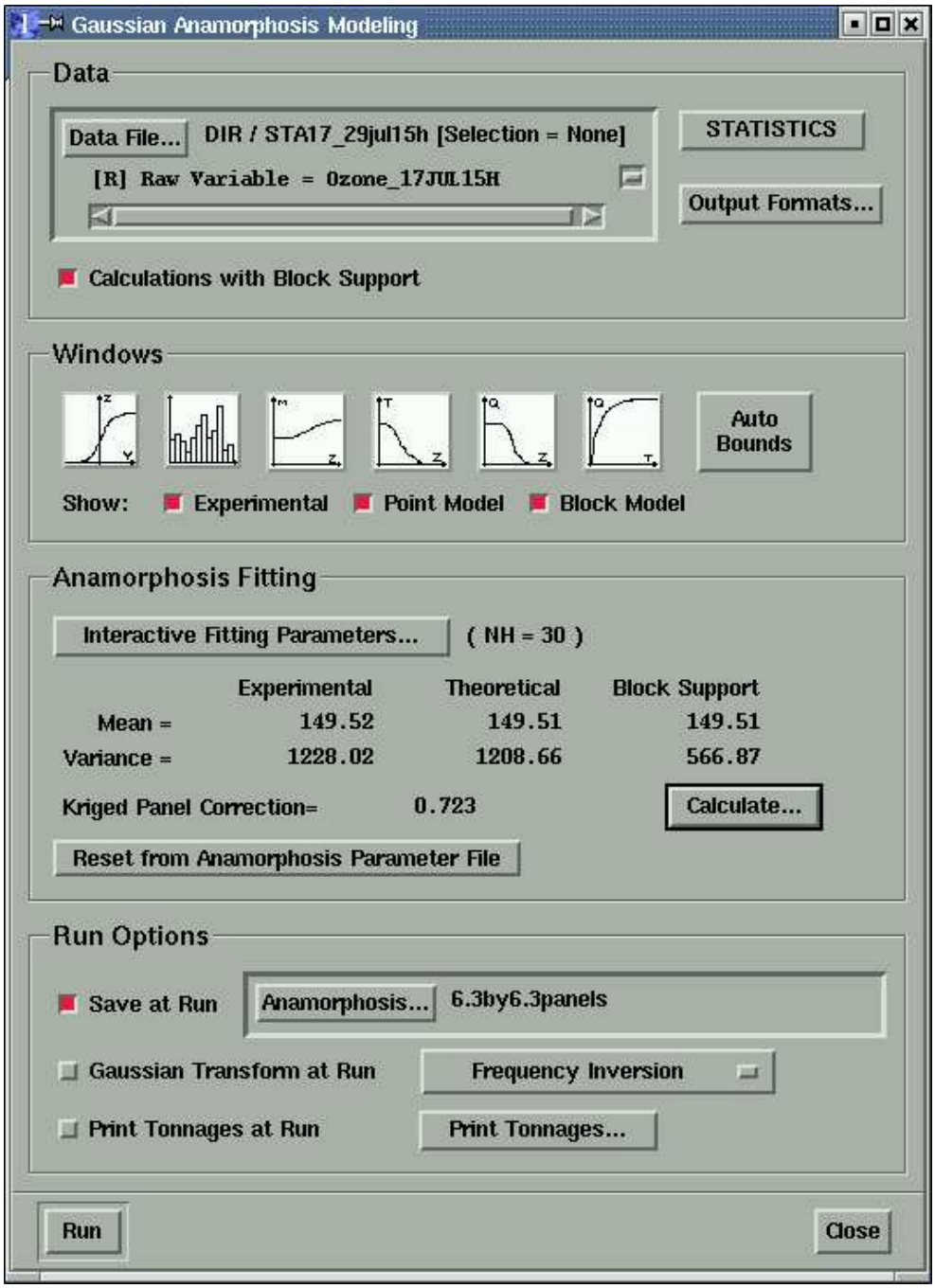

Figure 2.4: Isatis window for the anamorphosis with change-of-support for cell averages.

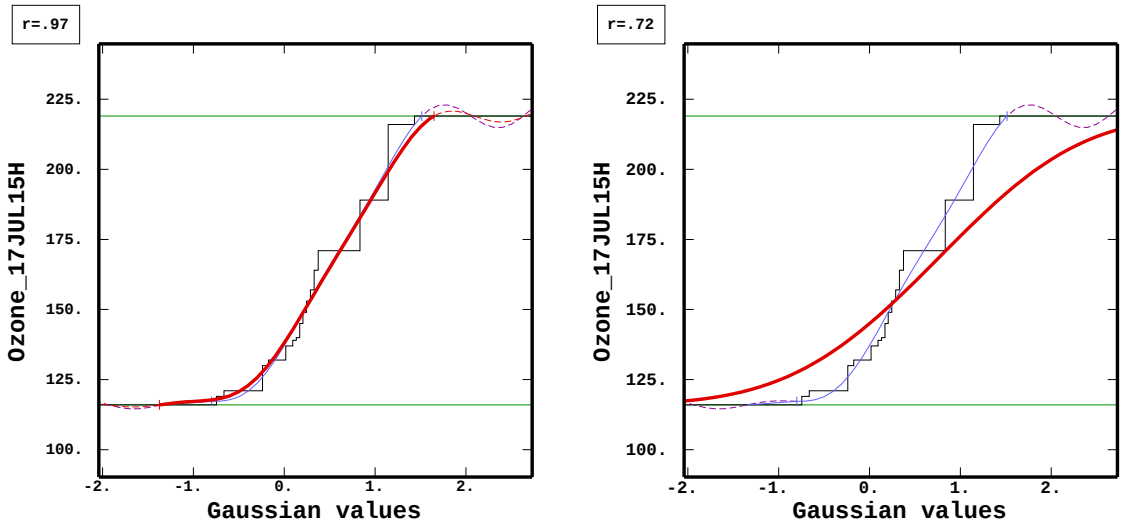

Figure 2.5: Point-block (left) and the point-cell (right) anamorphosis.

2.3 Proportion of Ile-de-France above air pollution alert level

The air pollution threshold for 1h ozone averages varies considerably in regulations of different countries of the world [4]. As an exercise we picked out a Swiss threshold of 120 μg/m^3 and the European threshold[5] of 180 μg/m^3.

We use the *uniform conditioning* [6, 11, 15] technique which consists in computing the expectation of the proportion of blocks above a threshold conditional to the cell value (computed by KED in Section 1.7). The uniform conditioning Isatis window obtained from the Isatis main window by

`Interpolation` $\mapsto$ `Estimation` $\mapsto$ `Uniform Conditioning`

is displayed on **Figure 2.6**. The input are the KED cell values stored under the name "`Ozon2`" as well as the parameter sets "`1.05by1.05 blocks`" and "`6.3by6.3 panels`" describing the discrete Gaussian point-block-cell change of support model. We ask for the three `cut-offs`:

$$[0, +\infty[, \quad [120, +\infty[, \quad [180, +\infty[$$

and store the output of uniform conditioning under the generic name "`UC`".

The quantity we are interested in, the proportion of blocks above threshold, is handled in Isatis as the *tonnage* (mining terminology) and is stored under the name `UC_T` for each cut-off. The maps corresponding to the alert levels generated with GMT in longitude and latitude

[4] For a recent survey of air pollution regulations and air quality indices see [4].

[5] European directive 92/72/CEE of 21.09.1992 according to [4].

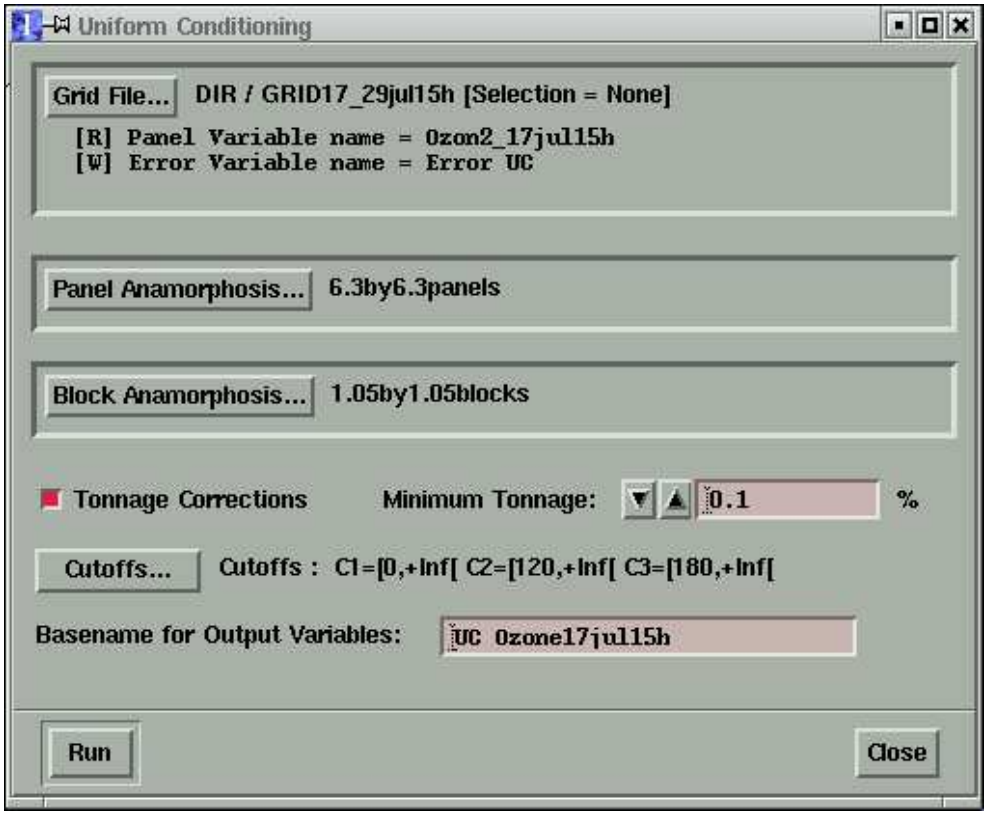

Figure 2.6: Isatis window for evaluating the proportion of blocks within Chimere cells above different pollution alert levels by uniform conditioning.

coordinates are displayed on **Figure 2.7**. With the Swiss air pollution threshold we would choose to inform the population for the whole Paris area as the proportion of square kilometer blocks above 120 μg/m^3 is more than 0.5 for most of the Ile-de-France. On the basis of the European threshold of 180 μg/m^3 we would decide however to warn only the population in the NW part of Ile-de-France.

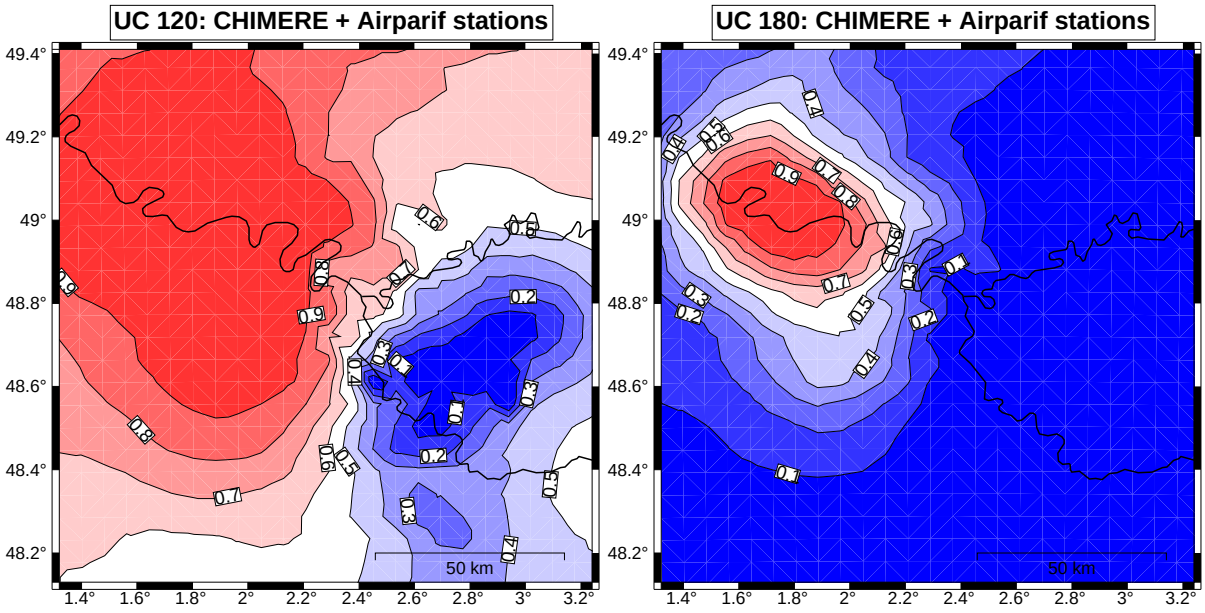

Figure 2.7: Proportion of square kilometer blocks within Ile-de-France above the Swiss (left) or the European (right) air pollution alert level.

Chapter 3

Conclusion

Automatic air pollution stations taking hourly measurements represent an important financial effort and their spatial coverage will necessarily remain low. A chemical transport model like Chimere, driven by meteorological predictions and an emissions inventory, advantageously supplements the station measurements, in particular because of its exhaustive coverage of space.

In the first part of this report the Chimere transport model output is used to capture the non-stationarity of a probabilistic model which postulates the presence of an ozone plume NW of Paris on a summer day of 1999. The spatial covariance is determined by calculating the experimental variogram in the direction which is least perturbed by drift, that is approximatively the NE-SW direction. Due to the small number of station measurements, the experimental variogram leaves some latitude in its interpretation and so two different isotropic models were fitted on the basis of the NE-SW sample variogram. New values of hourly ozone were computed for the Paris area through a kriging of the Airparif measurements in which the Chimere output acts as external drift. The results obtained with the second variogram model were kept for use in the second part of the study.

In the second part of the report the station measurements are considered explicitly as *point* values as compared to the Chimere 6.3×6.3 km^2 *cell* averages. A discrete Gaussian change-of-support model is built using the Airparif values and the corrected Chimere output from the first part. A new spatial decision unit is introduced in the form of *blocks* of square kilometer size, i.e. each Chimere cell is subdivided into 6×6 blocks. The motivation is to provide the decision maker with a smaller spatial unit than the Chimere cells and this is done by setting up a *point-block-cell* change-of-support model.

Two alert thresholds (120 and 180 μg/m^{3}ozone) stemming respectively from a Swiss and a European air pollution regulation are applied in a uniform conditioning of the block statistics by Chimere cell averages. The final product of the case study is an estimate of the proportion of blocks within each Chimere cell which are above a specific ozone threshold. Results are presented in the form of contour maps for the Swiss and the European air pollution thresholds. They represent a spatial normalization of station and transport model output in a form easy to

handle by a decision maker. The type of decision that could be taken is discussed, leading to different actions depending on whether either the Swiss or the European threshold has normative value.

The report contains detailed technical comments about the implementation of such a case study with the geostatistical software Isatis, which is widely available in the community of air pollution authorities (at least in France).

Acknowledgments

This work has been performed within the framework of the European project "IMPACT", contract IST-1999-11313. Discussions with Chris Roth from Airparif, Nadège Blond and Robert Vautard from LMD (Ecole Polytechnique) were of great benefit. Jacques Deraisme and Nicolas Jeannée from Géovariances provided a yet unpublished new chapter of the Isatis documentation about the application of non-linear geostatistics (using the Walker lake data) which served as a source of inspiration. Didier Renard from Centre de Géostatistique usefully commented a draft version of the manuscript.

Bibliography

[1] BERTINO, L., AND WACKERNAGEL, H. Case studies of change-of-support problems. Tech. Rep. N–21/02/G, Centre de Géostatistique, Ecole des Mines de Paris, Fontainebleau, 2002. (Downloadable from: http://www.mai.liu.se/impact/).

[2] BLEINES, C., PERSEVAL, S., RAMBERT, F., RENARD, D., AND TOUFFAIT, Y. *Isatis Software Manual*. Géovariances & Ecole des Mines de Paris, Avon, March 2000.

[3] BLOND, N. *Assimilation de Données Photochimiques et Prévision de la Pollution Troposphérique*. Doctoral thesis, Ecole Polytechnique, 2002.

[4] GARCIA, J., COLOSIO, J., AND JAMET, P. *Les indices de qualité de l'air: élaboration, usages et comparaisons internationales*. Les Presses de l'Ecole des Mines, Paris, 2001.

[5] GRIMVALL, A., WACKERNAGEL, H., AND LAJAUNIE, C. Normalisation of environmental quality data. In *Sustainability in the Information Society* (Marburg, 2001), L. M. Hilty and P. W. Gilgen, Eds., Metropolis-Verlag, pp. 583–590.

[6] GUIBAL, D., AND REMACRE, A. Local estimation of the recoverable reserves: comparing various methods with the reality on a porphyry copper deposit. In Verly et al. [14], pp. 435–448.

[7] HUDSON, G., AND WACKERNAGEL, H. Mapping temperature using kriging with external drift: theory and an example from Scotland. *International J. Climatology 14* (1994), 77–91.

[8] LAJAUNIE, C., AND WACKERNAGEL, H. Geostatistical approaches to change of support problems: Theoretical framework. Tech. Rep. N–30/01/G, Centre de Géostatistique, Ecole des Mines de Paris, Fontainebleau, 2000. (Downloadable from: http://www.mai.liu.se/impact/).

[9] LAJAUNIE, C., AND WACKERNAGEL, H. Geostatistical normalization: Theoretical framework. Tech. Rep. N–29/01/G, Centre de Géostatistique, Ecole des Mines de Paris, Fontainebleau, 2000. (Downloadable from: http://www.mai.liu.se/impact/).

[10] LAJAUNIE, C., WACKERNAGEL, H., AND BERTINO, L. Geostatistical normalization: Case studies. Tech. Rep. N–31/01/G, Centre de Géostatistique, Ecole des Mines de Paris, Fontainebleau, 2001. (Downloadable from: http://www.mai.liu.se/impact/).

[11] RIVOIRARD, J. *Introduction to Disjunctive Kriging and Non-Linear Geostatistics*. Oxford University Press, Oxford, 1994.

[12] SCHMIDT, H., DEROGNAT, C., VAUTARD, R., AND BEEKMANN, M. A comparison of simulated and observed ozone mixing ratios for the summer of 1998 in western Europe. *Atmospheric Environment 35* (2001), 6277–6297.

[13] VAUTARD, R., BEEKMANN, M., ROUX, J., AND GOMBERT, D. Validation of a deterministic forecasting system for the ozone concentrations over the Paris area. *Atmospheric Environment 35* (2001), 2449–2461.

[14] VERLY, G., DAVID, M., AND JOURNEL, A. G., Eds. *Geostatistics for Natural Resources Characterization*, vol. C-122 of *NATO ASI Series*. Reidel, Dordrecht, 1984.

[15] WACKERNAGEL, H. *Multivariate Geostatistics: an Introduction with Applications*, 3rd ed. Springer-Verlag, Berlin, 2003.